Carbon Letters (2022) 32:713–726
https://doi.org/10.1007/s42823-022-00320-2

Online ISSN 2233-4998
Print ISSN 1976-4251

REVIEW

Flexible piezoresistive strain sensor based on CNTs–polymer composites: a brief review

Ying Yi[1] · Bo Wang[2] · Xingyue Liu[1] · Changping Li[3]

Received: 18 October 2021 / Revised: 15 December 2021 / Accepted: 30 December 2021 / Published online: 8 February 2022

Abstract
This article presents recent advancements in the development of flexible piezoresistive strain sensors based on carbon nanotubes (CNTs)–polymer composites, with particular attention to their electromechanical properties. Various fabrication approaches and material preparation of CNTs–polymer composites with improved piezoresistive performance are introduced. Moreover, the article presents the working principle of the piezoresistive sensors in terms of the tunneling effect and disconnection-reconnection mechanism. The sensing performances of recently reported applications are studied. This work also reveals that the CNTs–polymer composites have great potential for flexible, skin-mountable, and wearable electronics applications. Finally, possible challenges for the future developments of CNTs–polymer composites are discussed.

Keywords CNT · Strain sensor · Polymer sensor

1 Introduction

Piezoresistive material-based strain sensors have been intensively used in, such as wearable electronics [1–3], displacement detection [4], physiological monitoring [5], and dosage surveillance [6]. Among the reported piezoresistive materials, carbon nanotubes (CNTs) that were first reported in the 1990s [7–9] have attracted growing interest in recent years. They possess superior properties, such as electrical, mechanical, optical, and chemical properties; their strength is over tenfold larger compared to the other industrial fibers. The characteristics of some piezoresistive materials against CNTs are summarized in Table 1 [10]. CNTs are seamless cylindrical structures of single or multiple layers of graphene, denoted as single-wall CNTs (SWNTs) or multi-wall CNTs (MWNTs), respectively. The structures of SWNTs and MWNTs are depicted in Fig. 1. SWNCTs are cylinder-like structured which are formed through a single sheet of graphene rolled seamlessly; it has a diameter of 1–2 nm and length of up to centimeters. MWCNTs consist of multiple concentric SWNCTs which are separated by about 0.35 nm. SWNTs usually have higher electrical conductivity (10^6 S/cm) and thermal conductivity (~3500 W/mK) than MWNTs (3×10^4 S/cm, 3000 W/mK), been acting as a metallic role. As a common piezoresistive strain sensor type, CNTs–polymer composites that change in electrical resistance upon an external force (namely piezoresistive effects) have gained popularity [11].

The piezoresistive characteristics of CNTs-filled polymer composites were demonstrated in [19, 20], and they were introduced comprehensively in [21, 22] as strain sensors. The works aforementioned mainly focused on the relationship between the applied pressure and resistance change of the composites. On the other hand, the piezoresistive mechanism of the CNTs–polymer composites should be more comprehensively studied from the view of the changes in the micro-scale. A 3D statistical resistor network model was introduced to simulate the resistance change when the strain was applied to MWNTs-filled polymer composites [23]. Different piezoresistive properties can be found in CNTs–polymer composites with different polymer matrixes [21]. The piezoresistivity of conductive polymer composite

✉ Changping Li
licp@cqupt.edu.cn

1 School of Mechanical Engineering and Electronic Information, China University of Geosciences, Wuhan, China

2 Division of Information and Computing Technology, College of Science and Engineering, Hamad Bin Khalifa University, Doha, Qatar

3 College of Communication and Information Engineering, Chongqing University of Posts and Telecommunications, Chongqing, China

Table 1 Characteristics comparison between the CNTs and other materials

	Thermal conductivity, (W/m K)	Mechanical		Resistivity, (10^{-2} μΩm)	Refs
		Tensile strength (GPa)	Young's modulus (GPa)		
Carbon nanotube (SWCNTs)	3000	50–500	1000	0.05–0.5	[12, 13]
Carbon nanotube (MWCNTs)	3000	10–60	300–1000	0.05–0.5	
Graphene	200–2000	130	1000	0.01	[14, 15]
Graphite	100–400	0.013–0.07	4.1–27.6	0.3–6	[16]
Copper	400	0.21–0.53	121–133	1.72	[17]
Silver	450	0.11–0.34	69–74	1.59	[18]
Gold	345	0.13–0.2	79	2.24	[18]

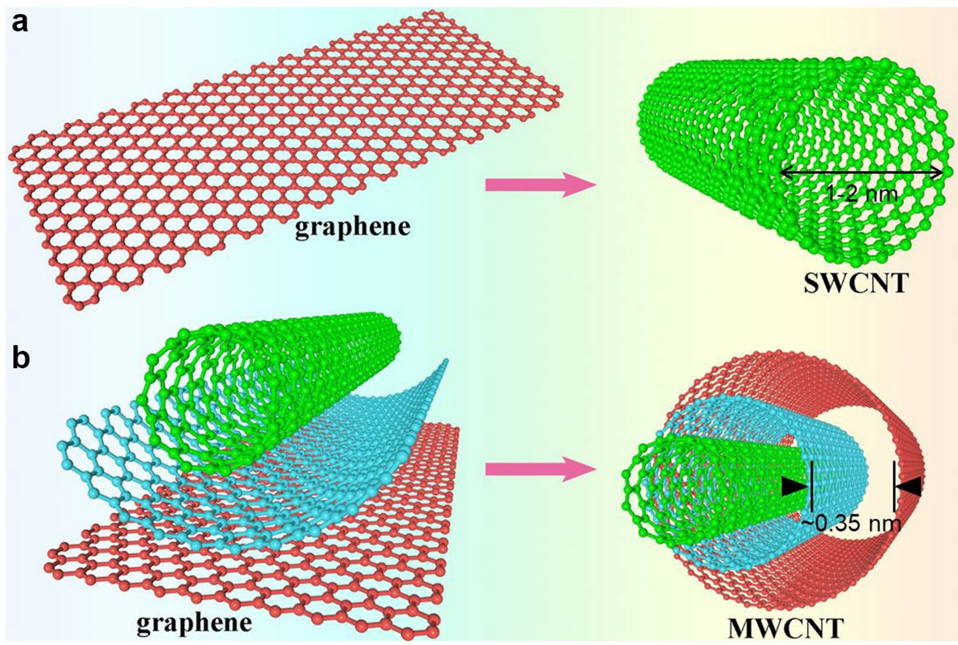

Fig. 1 **A** Structure of SWNTs. **B** Structure of MWNTs

that used CNT and silicon rubber was analyzed in terms of the change in the conductive network [24]. CNTs can be more easily embedded into polymer composite structures for in situ measurement than the other traditional strain sensor materials. The CNTs have a high aspect ratio, their diameter usually does not exceed 100 nm, and the length can achieve up to hundreds of millimeters, which exhibits a 1D nanostructure. Consequently, the CNTs are usually filled in polymers to form an effective conductive network in a composite with a 3D structure. The piezoresistivity and conductivity of CNTs–polymer composites were investigated in [25–29]; in such composites, CNTs were used in their conductive phase, while the polymer performed as insulation. The optimal ratio of the CNTs is about 2 vol% (the volume fraction) [24], and the high ratio will cause the deterioration of the mechanical property of the entire composites, while decreasing the ratio of CNTs will lead to increased resistance, making the integration of the other circuit systems difficult.

This paper aims to survey fabrication processes, working principles, and sensor applications of the CNTs–polymer composites. The article is organized as follows: the second section summarizes novel approaches and functional nano-materials for the fabrication of flexible CNTs–polymer composites in detail; in the third section, the mechanisms involved in the strain-responsive behavior of piezoresistive-type sensors are explained; the fourth section introduces elastic and sensitive strain sensors that commonly serve as E-skin; the next section discusses possible challenges for the skin-mountable and wearable sensor applications; the last section gives the conclusion points.

2 Fabrication processes

The CNTs–polymer composites are in general fabricated by either direct mixing of the CNT and polymer in a suitable solvent [30–32], melt processing of bulk composite [33, 34], melt processing of composite fibers [35, 36], polymerization [37–39], or coagulation spinning of composites [40–42]. However, it is challenging that pristine CNTs cannot be well dispersed in most solvents; thus, the performance of the CNTs–polymer composites is greatly degraded following the traditional fabrication procedures. Recently, new approaches for uniform distribution of the CNTs in the polymer have been investigated; the spinning approaches, dispersion conditions, and characterizations of various CNTs–polymer composites are summarized in Table 2. A layer-by-layer approach that involves building up a layered composite film by alternate dipping of a substrate into the dispersion of CNTs and polyelectrolyte solution was introduced in [43, 44]. The major merits of this approach include controllable thickness and polymer–nanotube ratio and high nanotube loading level. The swelling technique is another promising post-processing approach that enables the incorporation of CNTs into insoluble or temperature-sensitive polymers. For example, MWNTs-Kevlar and MWNTs-polyethylene (PE) composites can be produced by swelling Kevlar fibers and PE film in a suspension of MWNTs in N-methylpyrrolidone (NMP) [45] and tetrahydrofuran (THF) [46] under ultra-sonication. The resulting composites exhibit

Table 2 Summary of CNT–polymer composites fabrication approaches and their key characteristics

Polymer	Spinning method	CNT dispersion method	CNT type	wt_{max} (wt%)	Property improved by the addition of CNTs?			Refs
					Tensile property	Electrical conductivity	Thermal transition	
PAN	Gel		S, M	5	Y		Y	[51]
PE		Melt mixing	M	5	Y		Y	[52]
PVA	Mel	Surfactant + sonication	S, M	1	Y	Y		[53]
	Coag	Surfactant + sonication	M	11		Y		[54]
PA		Melt mixing	M	2	Y	Y		[55]
PMMA	Melt	Dry mixing → melt mixing	C	10	Y		Y	[56]
PET		Melt mixing	S	1	Y		Y	[57]
Pitch	Melt	Melt mixing	M	0.3	Y		Y	[58]
		Sonication, evaporation	S	10	Y	Y		[59]
PAni	Wet	Poly-sol + sonication	S	2	Y	Y		[60]
PP			M	1	Y		Y	[61]
Lignin	elec	Co-solvent + sonication	M	6	Y	Y		[62]
PEK	DJ-wet	In situ	F	20	Y	Y	Y	[63]
PEI	coag	Aqueous + surfactant + sonication	S	75	Y	Y	Y	[64]
PVP	elec	Poly-sol + sonication	M	4		Y	Y	[65]
PI	melt	Melt mixing	S	1	Y			[66]
PBT	elect	Sonication	M	4	Y		Y	[67]
PAni + PP	melt	Melt mixing	M	7.5		Y	Y	[68]
PP + PA	melt	Melt mixing	M	5	Y	Y	Y	[69]

Polymer abbreviations: polyacrylonitrile (PAN); polyethylene (PE); poly(vinyl alcohol) (PVA); polyamide (PA); poly(methyl methacrylate) (PMMA); polyethylene terephthalate (PET); polyaniline (PAni); polypropylene (PP); poly(ether ketone) (PEK); polyethyleneimine (PEI); polyvinylpyrrolidone (PVP); polyimide (PI); poly(polybutylece terephthalate) (PBT)

Spinning method abbreviations: gel-spinning (gel.); melt-spinning (melt.); wet-spinning (wet.); coagulation spinning (coag.); electro-spinning (elec.); dry-jet wet-spinning (DJ-wet.)

Method abbreviations: melt mixing, the polymer is melt by twin-screw, melt mixer or the other mechanical methods, and then, it is mixed with the CNTs; surfactant + sonication, surfactants are used to disperse CNTs in a solvent that facilitates ultra-sonication treatment of polymers; evaporation, dispersing the CNT in a solvent which works for both CNT and polymer by ultra-sonication, the polymer solution is then mixed with the solvent after the CNT dispersion. The solvent can be removed by evaporation, leaving the CNT–polymer with the required concentration; poly-sol, CNTs are dispersed in a solvent that is capable of being dissolving polymer but poor for CNTs; co-solvent, CNTs are dispersed in a solvent that works for both CNTs and polymer; in situ, in situ polymerizations of CNTs with polymer

CNT type: S, SWNT; F, few wall nanotubes; M, MWNT; C, carbon nano-fiber higher electrical conductivity and mechanical ability. The bucky-paper-based approach has been extensively reported [47–49] to produce a thin porous assembly of CNTs. The fabricated composites normally have a laminar structure with a random orientation of the bundles of tubes in the plane of the sheet [50].

The other functional nano-particles that can be added into the CNTs–polymer to improve the sensing performance include the following: in [70], the silver nano-particles (AgNPs) were added in the polymer composites to prevent the intact interaction between neighboring CNTs as well as tailor the conductive pathways in the composite; Fe_3O_4 nano-particles were mixed with CNTs-Poly (vinylidene fluoride) (PVDF) to improve the thermal conductivity of the composites, which in turn converted microwave energy into Joule heating systems [71]. In this review, the composites that are formed by mixing the CNTs and the polymer and their corresponding fundamental structure are emphasized. Regarding support materials for the CNTs, silicone-based elastomers [e.g., polydimethylsiloxane (PDMS)] [72–76] and rubbers [77–79] are widely used. Figure 2 illustrates an overall fabrication process of a popular CNTs–polymer reported in [80], and it is composed of MWNTs, PDMS, and reverse micelle solution (RMS). The components and their weight ratio are given in Fig. 2a. RMS solution is formed after ultrasonic vibration of 30 min and the mechanical stirring for another 30 min until it becomes a homogeneous black gel-like solution (Fig. 2b), so that MWNTs can be able

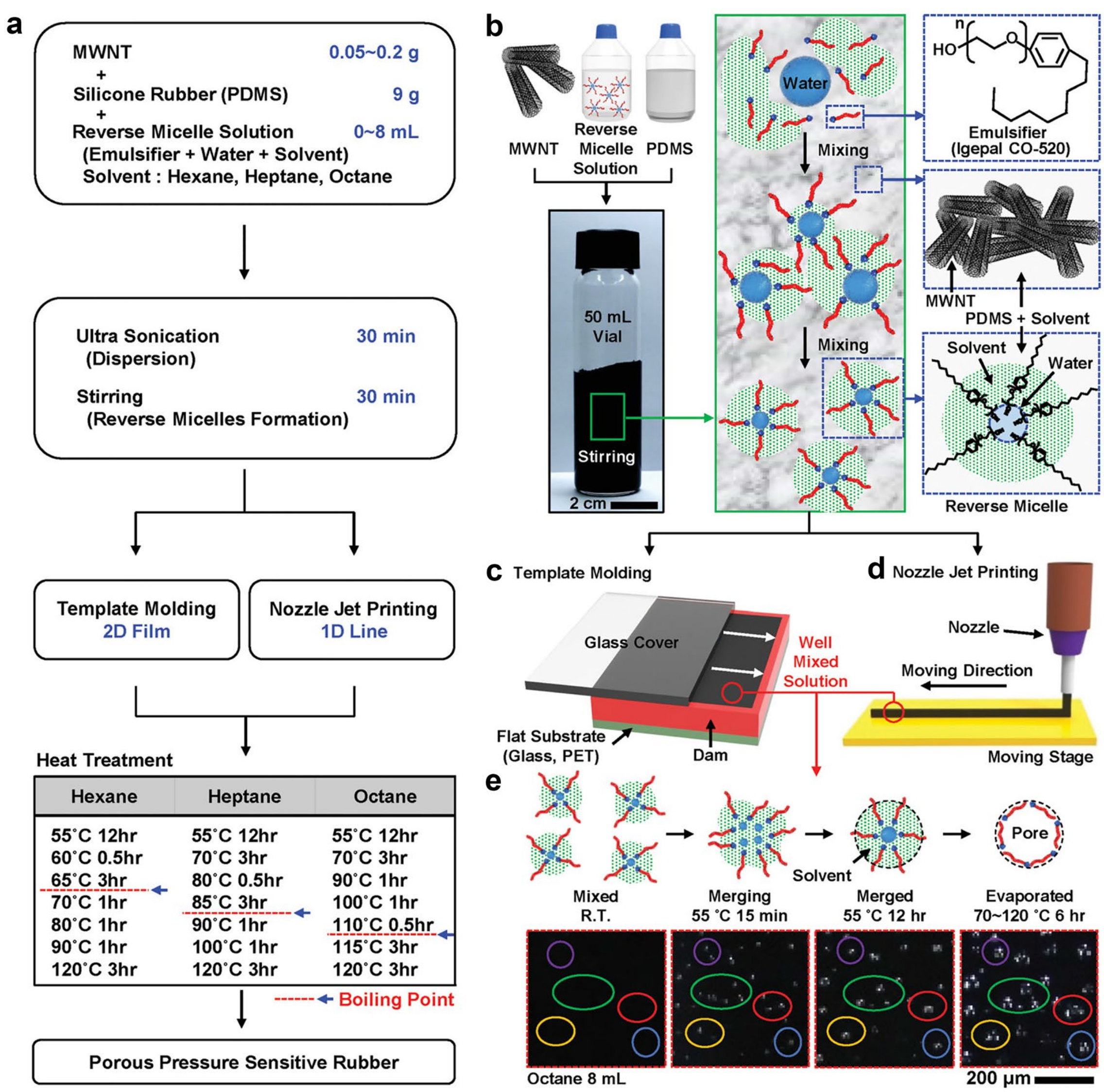

Fig. 2 **a** The flowchart of the fabrication process of flexible WMNTs-based strain sensor. **b** Illustration of mixing procedure. **c** The flat thin strain sensor film formation method. **d** The line pattern formed using the nozzle-jet printing method. **e** RMS behaviors during the heat treatment procedure [80]

to be evenly distributed to form a uniform RMS-MWNTs solution. The mixture of PDMS and RMS-MWNTs then is poured into a flat and enclosed substrate to form a film (Fig. 2c).

Nozzle-jet printing is used on the target substrate to design various line patterns (Fig. 2d). The final step is to cure the PDMS and solidify the mixture. The temperature for the process follows the heating-treatment requirement as listed at the bottom of Fig. 2(a). The reverse micelles had evaporated, producing a porous structure during the heating process. The more MWNTs were mixed, and the smaller pores were formed (Fig. 2e). Computer-aided design (CAD) can also be used in the nozzle-jet-printing for line pattern, as depicted in Fig. 3 [80]. MWNTs mixed-rubber solution was patterned by moderating the flow rates and the nozzle movement speeds after patterning is done. Silicone oil was used to cover the rubber solution, because it was immiscible with RMS and does not damage the pressure-sensitive rubber pattern. The rubber solution adhered to the flexible PET substrate, so the final strain sensor can suffer from numerous deformations, as shown in Fig. 3b. The magnified view of uniformly distributed pores is shown in Fig. 3c.

2.1 Strain-responsive principle

The structure of the piezoresistive sensor plays a critical role in the strain-responsive principle. The sensor was usually designed as a sandwich structure [81], double-percolation structure [82], porous structure [83], segregation structure [84], sponge structure [85], etc. [86]. In [87], a flexible piezoresistive sensor with an interlocked structure was explored as bionic human skin, to detect three-dimensional force; A piezoresistive membrane with a four-petal structure, was designed as a Wheatstone bridge, to be applied in low-pressure measurement applications [88]; The MWCNTs were assembled onto a polydimethylsiloxane (PDMS) film with a pyramidal microarray structure, to output tactile force signal [89]. In this review, the structure design of the sensor is not emphasized; only the working principle of the CNTs–polymer of which deformation results in electrical resistance change is analyzed.

An SEM image of the CNTs distribution in the polymer is shown in Fig. 4 [90]. It is observed that the conductive particles are randomly distributed and the adjacent CNTs

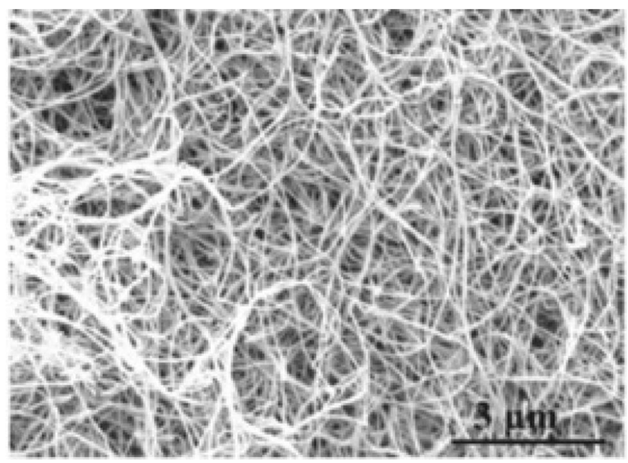

Fig. 4 SEM image of CNTs dispersion [90]

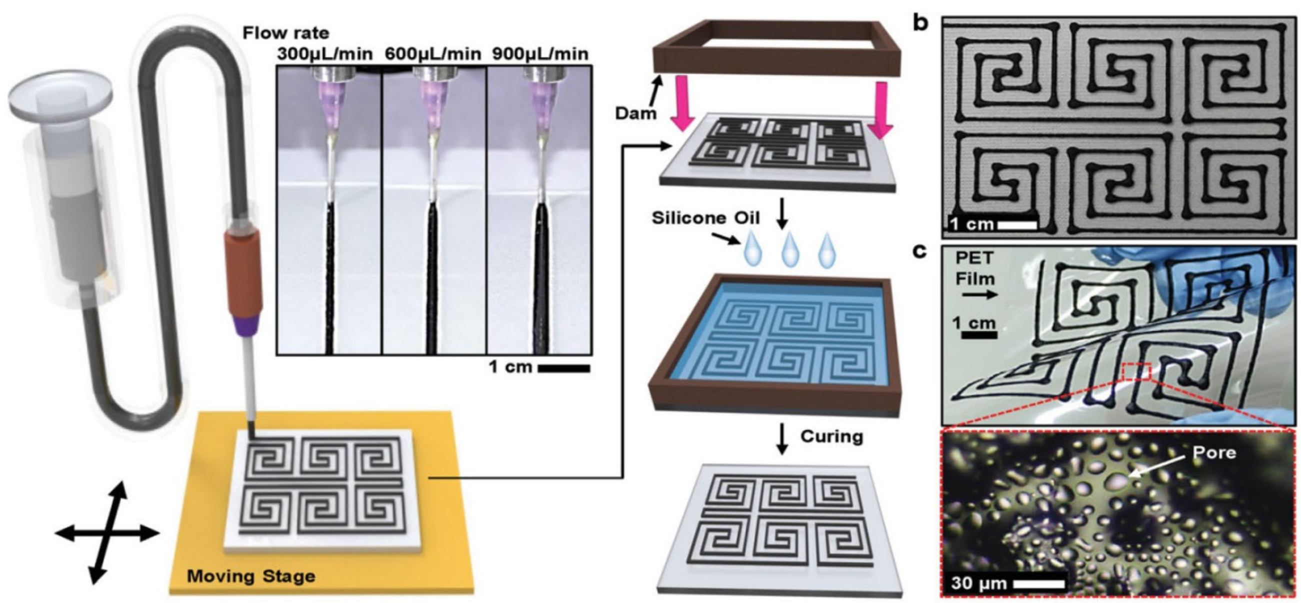

Fig. 3 Illustration of the nozzle-jet printing process for the patterned PPSR [80]

are insulated by thin polymer films. However, the tunneling transport of electrons can make the separated CNTs conductively connected through junction gaps, forming a conductive network [32]. The so-called "tunnel effect" demonstrates a phenomenon where the current can flow over adjacent conductive particles as long as their gaps are very small [91, 92]. Therefore, the tunnel effect is commonly presented to explain the conductivity of the CNTs–polymer [23, 93].

As shown in Fig. 5a, the whole resistance of the random CNTs network includes R_N of all the CNT segments, R_J of all the tunneling resistances due to the junctions. When the external force is applied on the CNTs-filled composite, the resistance of the composite will change, which refers to three possible reasons (Fig. 5b): (1) variation of R_J occurs due to the change of junction gap; (2) geometry deformation induced-CNT resistance variation $\Delta\rho_{CNT}$; (3) junction length along with CNTs changes Δl_{CNT} due to slippage. Reasons 2 and 3 contribute to the variation of R_N. Actually, for the CNTs–polymer composites, R_N does not dominate the resistance of the composites network, because R_N is usually far less as compared to R_J, and the effect of ΔR_N can nearly be ignored for the resistance variation of the composites. Therefore, the average junction gap variation (AJGV) is a quantitative parameter to mainly determine the piezoresistive performance of the network when the composite suffers from external strain or compression.

Because the conductivity of the composite is mainly based on the CNTs-formed conductive links, the entire resistance is mainly determined by the AJGV between the adjacent CNTs. Based on the tunneling effect theory, the tunneling current density J over the insulation gap can be given by [95]

$$J = \frac{3e^2 U\sqrt{2m\varphi}}{2h^2 d e^{4\pi h^{-1} d\sqrt{2m\varphi}}},$$

where U is applied voltage, d is the thickness of the insulation, φ means the height of the potential barrier, m is electron mass, e is electron charge, and h is Planck's constant. It can be observed that an increasing gap d between the neighbor CNTs caused by the stretching of the sensor leads to an increasing resistance change, while the decreased junction gap caused by compression will cause a decreasing resistance change.

Moreover, disconnection and reconnection of the CNTs-formed conductive links or the occurrence of cracks in the composites can also cause the resistance change during deforming the sensor [96]. Figure 6 illustrates a cracked

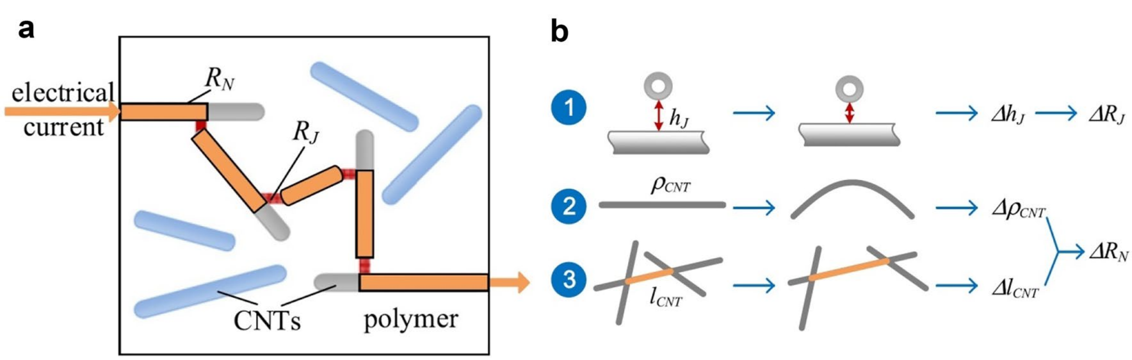

Fig. 5 Schematic illustration of **a** an electrical conductive CNTs in a polymer matrix, and **b** three possible reasons for the piezoresistive effect [94]

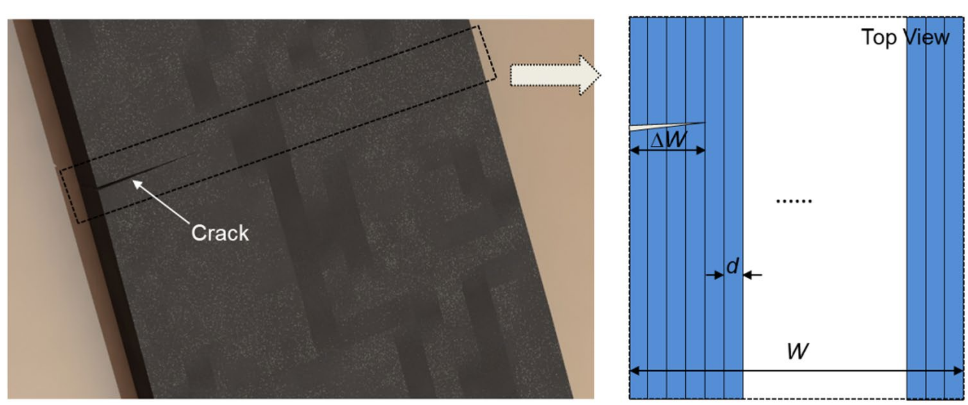

Fig. 6 Illustration of the effective conductive pathways and cracked surface of the polymer composites

surface of the conductive polymer composites containing CNTs and the concept of the effective conductive pathways. It is assumed that the initial region can be divided into N_0 identical conductive pathways [97] with a width d, the initial electrical resistance R_0 of the composite specimen, and its whole width W can be expressed by

$$\begin{cases} R_0 = R^E/N_0 \\ W = \sum_{i=1}^{N_0} d \end{cases},$$

where R^E denotes an effective resistance of a single conductive pathway. When the cracks occur and its propagation breaks effective conductive pathways, the crack extension ΔW can be obtained as follows:

$$\Delta W = W - \sum_{i=1}^{N'} d,$$

where N' is the number of effective conductive pathways after crack propagation. Then, the resistance of the composite specimen becomes

$$R' = R^E/N'.$$

Thus, the change in the resistance of the composite specimen, $\Delta R = R'\text{-}R_0$, can be approximately regarded in terms of ΔW and W as

$$\Delta R = \frac{\Delta W}{W - \Delta W} \cdot R_0.$$

Therefore, the crack extension ΔW caused by the external force or deformation of the polymer composites causes an increasing resistance change ΔR, explaining the principle of the sensors which are based on the change in contact resistance between the cracked fracture structures.

To clarify the relationship between the strain and resistance, Fig. 7a shows a basic setup for measuring the electrical

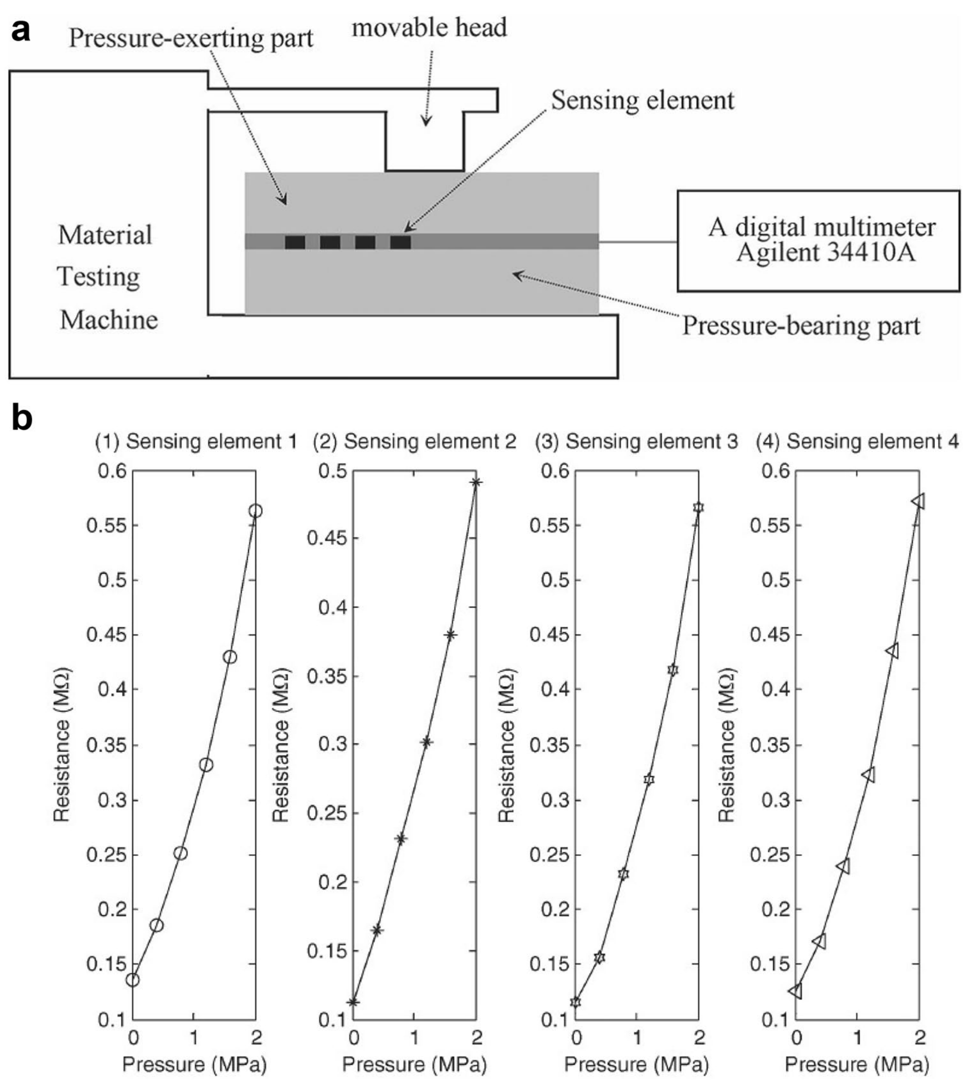

Fig. 7 **a** The measurement setup for sensing the electrical resistance under different applied pressures [24]; **b** resistance–pressure curves of the four sensing elements [24]

resistance of the sensing element under different levels of pressure. The material testing machine can apply pressure on the testing material by controlling the movement of the movable head. The resistance is recorded by a digital multimeter with the applied pressure. When the external force is applied to the CNTs–polymer composites, the distance between separated CNTs will change accordingly. If the gap is reduced to a threshold range where the tunneling effect can be able to happen, a new conductive path can be formed, so that the current can be able to penetrate the insulating matrix. Accordingly, the formation or destruction of the effective conductive paths may change the actual number of the conductive links, so the resistance of the entire composites changes based on the AJGV between the adjacent CNTs in the conductive network. Specifically, external pressure may make the CNTs move far away from each other, decreasing the number of effective conductive paths; this, in turn, increases the resistance. Figure 7b shows that the resistance increases with the increase of pressure for four different tested elements. This result convicts that the compression enlarges the gap between carbon nanotubes and reduces the number of effective conductive paths, resulting in destruction effects at conductive links.

2.2 Applications

Flexible pressure (or strain)-sensitive CNTs–polymer composites can be used in a variety of engineering fields. The most promising applications include wearable electronics, robotic skins, and medical health monitoring [98]. In this section, the sensors based on CNTs–polymer composites that serve as skin-mountable strain gauges are emphasized, for example, the electronic-skin (E-skin). In general, the resistance or capacitance of the sensor that deploys at the skin surface or joints changes when it deforms. Human physiological signals and real-time wrist pulse detection can be monitored according to the output signal of the sensor. Owing to the excellent sensing performance of the sensor in terms of rapid response time, great stability, and repeatability, the E-skin can work in conjunction with the wearable device for the prevention and prediction of illnesses. As shown in Fig. 8, a flexible pressure-sensitive polymer film based on the MWNTs adhered to the wrist, the geometry of the film changed correspondingly for the deformation of the skin surface; consequently, the film was stretched and bent. The two insets on the right of Fig. 8 show the resistance variations of a wearable sensor according to different bending frequencies. Therefore, the repetitive bending motions of the human wrist can be monitored by doing so, and the cyclic tests did not induce any unwanted signal and material degradation, exhibiting a stable working performance.

As well known, speech can cause the deformation of the epidermis and muscles around the throat; therefore, E-skin can be able to provide a novel and achievable application for voice recognition. Figure 9a shows a prototype of a strain sensor-based E-skin; it can be used for monitoring pressure difference at a person's neck during voicing, because the resistance would change corresponding to the muscle movement induced by speech. Figure 9b depicts different *I*–*t* profiles when the tester spoke different words. By doing so, different voices and speech can be recognized through fast and sensitive strain sensing. To investigate the point that the similar *I*–*t* curves can be repetitively obtained for speaking the same thing, saying "hello" and "one world one dream" three times and Fig. 9c, d shows the corresponding *I*–*t* curves, respectively. It is observed that the three *I*–*t* curves have nearly the same characteristic peaks and valleys, which convict the point aforementioned. This application can help those patients who damage their vocal cords recover their voicing ability via controlling their throat muscle movement.

A flexible pressure sensor can also provide great potential for modern biomedical applications. Figure 10 depicts a prototype of an MWNTs-based pressure sensor for detecting the wrist pulse. Wrist pulse can be able to indicate arterial

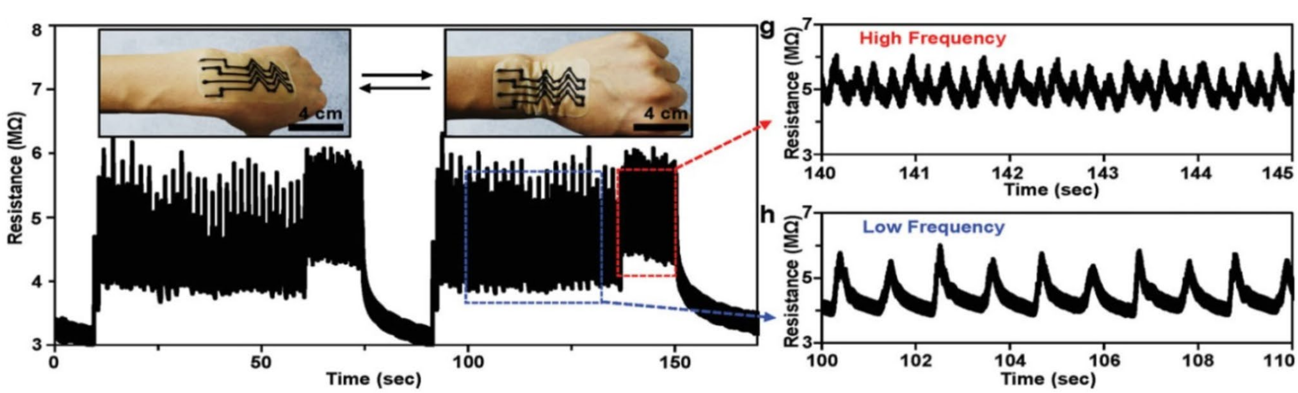

Fig. 8 Monitoring the resistance change according to the stretching and bending of the skin due to wrist movements; g–h) magnified views of measured signals for high-frequency and low-frequency movements [80]

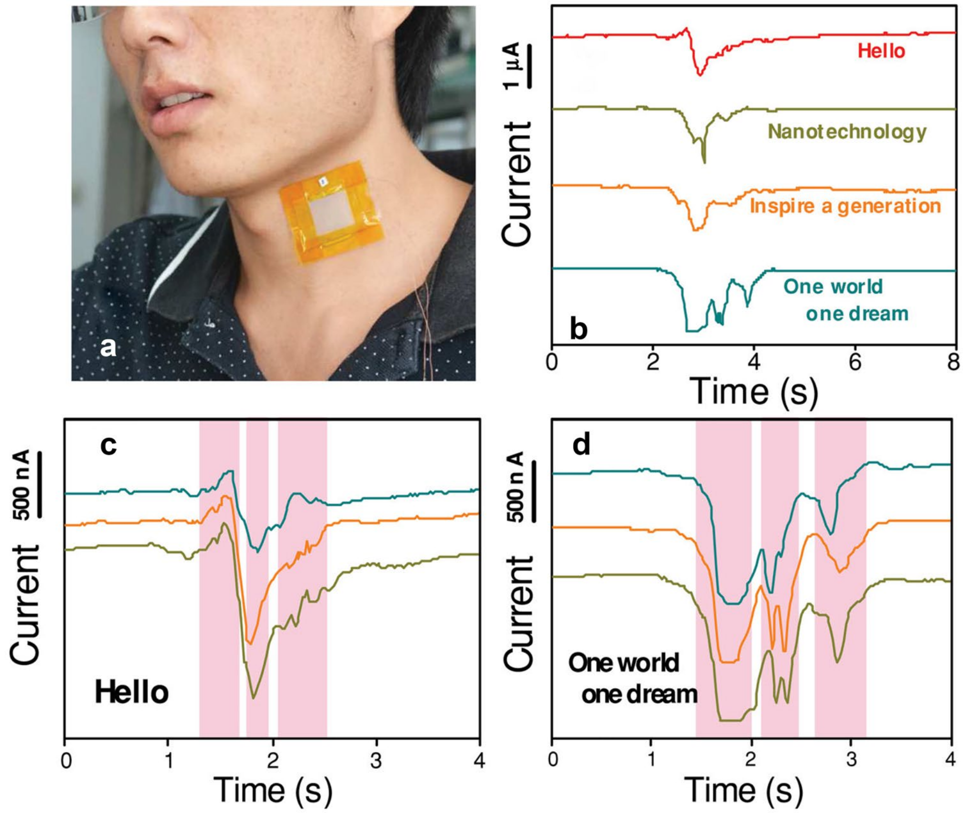

Fig. 9 **a** Prototype of E-skin directly adheres to a tester's neck for monitoring the muscle movement. **b**–**d** Real-time muscle movement monitor via *I*–*V* curves due to resistance change of flexible pressure sensor [99]

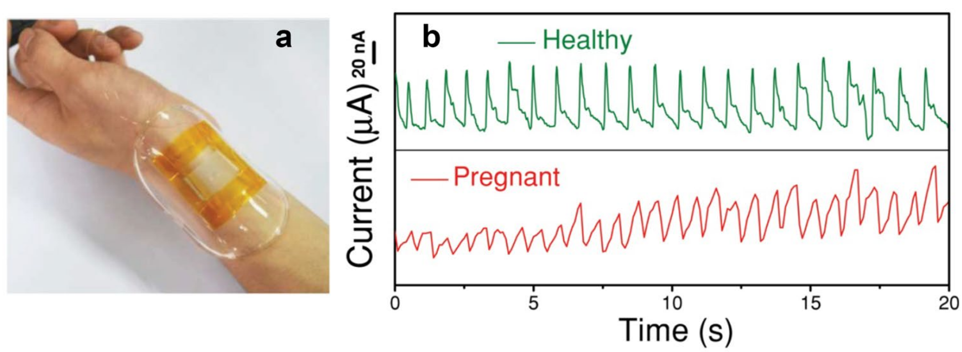

Fig. 10 **a** Prototype of electronic skin device fordetecting wrist pulses. **b** *I*–*V* curves demonstrate the wrist pulse of a healthy person and a pregnant-woman by using the pressure sensor [99]

blood pressure, heart rate, and other physiological information which helps the non-invasive medical diagnosis. For example, atherosclerosis can cause arterial pulse pathologic and affect arterial pressure, while wrist pulse is a key indicator to monitor arterial blood pressure, which can perform a rapid, easily operated, and effective method for diagnosing such cardiovascular diseases [100–102]. As shown in Fig. 10a, the pressure sensor that was placed on the wrist can differentiate the subtle pressure difference between those who are indifferent body conditions. Figure 10b provides two continuous *I*–*t* curves monitoring the wrist pulse for healthy people and a pregnant woman (21 weeks). It is seen that people with different body conditions owned different wrist pulse shapes and frequencies. The healthy person showed a regular and repeatable pulse shape, and the pulse frequency was 75 beats/min within a normal range. While, the pregnant woman showed an irregular pulse shape and intensity, and pulse frequency was 91 beats/min (out of the normal range).

As well known, speech can cause the deformation of the epidermis and muscles around the throat; therefore, E-skin can be able to provide a novel and achievable application for voice recognition. Figure 9a shows a prototype of a strain sensor-based E-skin; it can be used for monitoring pressure difference at a person's neck during voicing, because the resistance would change corresponding to the muscle movement induced by speech. Figure 9b depicts different *I*–*t* profiles when the tester spoke different words. By doing so, different voices and speech can be recognized through fast and sensitive strain sensing. To investigate the point that the similar *I–t* curves can be repetitively obtained for speaking the same thing, saying "hello" and "one world one dream" three times and Fig. 9c, d shows the corresponding *I–t* curves, respectively. It is observed that the three *I–t* curves have nearly the same characteristic peaks and valleys, which convict the point aforementioned. This application can help those patients who damage their vocal cords recover their voicing ability via controlling their throat muscle movement.

Figure 11 gives an example where a tank-like robot (MINDSTORMS NXT 2.0, LEGO, USA) was remotely controlled by a wearable sensor array. The instruction signals (moving forward, acceleration, deceleration, etc.) can be transmitted via the output voltage variation over each circuit. Figure 11a, b shows the images of piezoresistive sensors using MWNTs-filled polymer composites for detecting pressure and strain, respectively. The pressure sensor array consists of four channels, each of which functions different action command for controlling the motion of the robot. The strain sensors that were mounted on the middle and index fingers consist of two channels, triggering acceleration and deceleration, respectively. Each skin-mounted sensor was connected in series to a resistor of 100 kΩ (used as reference), and the six resistor-sensor pairs were connected in parallel. When a DC bias of 5 V was applied to the circuit, the output signals were measured from the point between the resistor and the

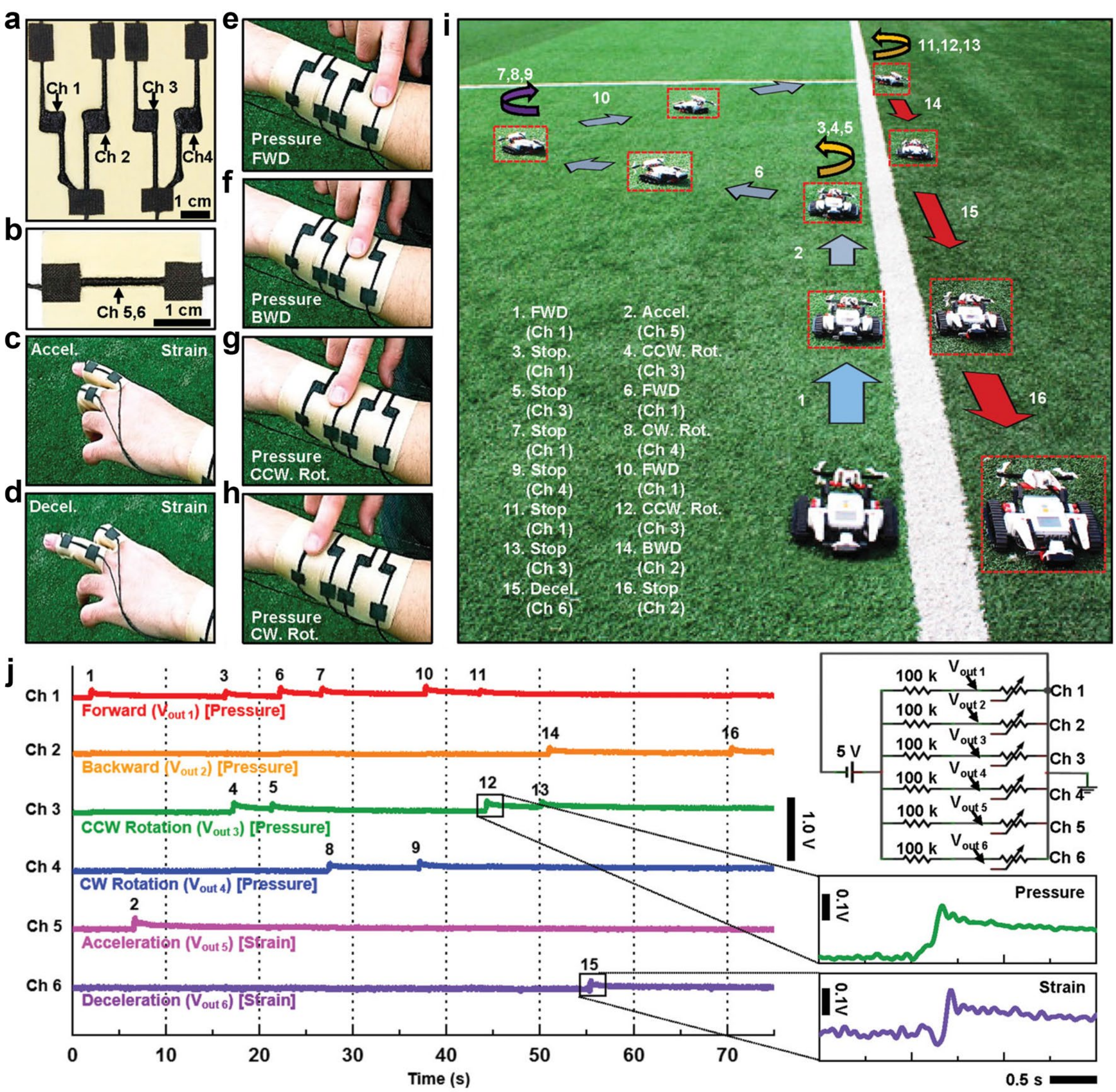

Fig. 11 Wearable mechanical sensor for remotely controlled applications. **A**–**I** images of flexible MWNTs-based strain sensors with different circuit structures. The respective functions of each sensor are displayed. **J** Output voltage signals from the sensor array while controlling the robot wirelessly [80]

sensor (Fig. 11j right top inset). The custom-made LabVIEW program analyzed the output signal changes of the six skin-mounted sensors induced by mechanical motions (e.g., pressing or stretching) and activated a specific keypad. The blue tooth embedded robot can receive the wireless signals and operate the corresponding instructions. Figure 11 provides an example for the human–machine interface (HMI) and convinces that the MWNTs-based sensor indeed exhibits a promising potential for HMI due to its high linearity and sensitivity. Actually, through this example, It can also be observed that CNTs used in tactile sensors own wider working ranges, low commercial cost, and less power consumption than optical, magnetic, ultrasonic materials. Their structures associated with read-out electronics are also simply deployed. For future applications, CNTs-based piezoresistive sensors can be widely used for humanoid robots or other healthcare control devices.

2.3 Discussion and challenges

Though CNTs–polymer composites-based strain sensor owns lots of advantages and offers great potential for a variety of applications, several challenges can still not be ignored. At least two significant issues need to be addressed here, including repeatability and stability.

- Repeatability: it refers to repeatable resistance change under cyclically applied strain. According to some latest studies, the resistance of CNTs–polymer composites shifts over time even an applied mechanical load is removed [103, 104]. This phenomenon will bring lots of serious problems in practical applications. Resistance drifting may attribute to breakdown and exfoliation of the surface of CNTs, as well as heat-induced by current passing through the conductive network.
- Stability: it denotes a stable resistance behavior over a long operation period. As for many piezoresistive strain sensors including CNTs, the *I*–*V* pulses are not similar to each other even the same strain is applied, inducing some precision issues. Moreover, owing to irreversible deterioration at interfaces of the CNTs and polymer composite, CNTs-based flexible strain sensors usually perform resistance hysteresis during cyclically operated strain loadings.

The selection of polymer is also an important factor. The weak polymer encapsulation is hard to sustain repeatable and permanent deformations and a high strain force (larger than 0.04%). Therefore, the fragility of the sensors is a critical issue that needs to be overcome.

3 Conclusion

The carbon nanotube is a popular material nowadays and exhibits a wide range of applications. Carbon nanotube-based pressure sensor with a flexible polymer composite shows promising trends in the field of tactile sensing, electronic-skin, and other human–machine interfaces. The working principle is mainly based on the tunneling theory which indicates that the resistance of the insulating phase is varying according to the geometry change. The sensing examples aforementioned demonstrate the feasibilities and high efficiency of the CNTs' conductive phase, paving the way to future healthcare monitoring, intelligent controlling devices.

Author contributions YY organized, modified, optimized, revised, and prepared the manuscript, BW summarized the Table 2, and XL drew Fig. 1 and summarized the Table 1. CL provided the content about the working principle in the section "Strain-Responsive Principle". All authors read and approved the final manuscript.

Funding This research received no external funding.

Declarations

Conflict of interest The authors declare no conflict of interest.

References

1. Gao L et al (2019) All paper-based flexible and wearable piezoresistive pressure sensor. ACS Appl Mater Interfaces 11(28):25034–25042
2. Sencadas V, Tawk C, Alici G (2020) Environmentally Friendly and Biodegradable Ultrasensitive Piezoresistive Sensors for Wearable Electronics Applications. ACS Appl Mater Interfaces 12(7):8761–8772
3. Chen Q et al (2018) Facile fabrication and performance of robust polymer/carbon nanotube coated spandex fibers for strain sensing. Compos A Appl Sci Manuf 112:186–196
4. Yi Y, Wang B, Bermak A (2019) A low-cost strain gauge displacement sensor fabricated via shadow mask printing. Sensors 19(21):4713
5. Zhang X et al (2021) High-performance flexible strain sensors based on biaxially stretched conductive polymer composites with carbon nanotubes immobilized on reduced graphene oxide. Compos Part A: Appl Sci Manuf 151:106665
6. Yi Y, Chiao M, Wang B (2021) An electrochemically actuated drug delivery device with in-situ dosage sensing. Smart Mater Struct 30(5):055003
7. Iijima S (1991) Helical microtubules of graphitic carbon. Nature 354(6348):56–58
8. Iijima S, Ichihashi T (1993) Single-shell carbon nanotubes of 1-nm diameter. Nature 363(6430):603–605
9. Bethune D et al (1993) Cobalt-catalysed growth of carbon nanotubes with single-atomic-layer walls. Nature 363(6430):605–607

10. Eshkalak SK et al (2017) A review on inkjet printing of CNT composites for smart applications. Appl Mater Today 9:372–386
11. Amjadi M et al (2016) Stretchable, skin-mountable, and wearable strain sensors and their potential applications: a review. Adv Funct Mater 26(11):1678–1698
12. Berber S, Kwon Y-K, Tománek D (2000) Unusually high thermal conductivity of carbon nanotubes. Phys Rev Lett 84(20):4613
13. Troiani H et al (2003) Direct observation of the mechanical properties of single-walled carbon nanotubes and their junctions at the atomic level. Nano Lett 3(6):751–755
14. Balandin AA (2011) Thermal properties of graphene and nanostructured carbon materials. Nat Mater 10(8):569–581
15. Lee C et al (2008) Measurement of the elastic properties and intrinsic strength of monolayer graphene. Science 321(5887):385–388
16. Klemens P, Pedraza D (1994) Thermal conductivity of graphite in the basal plane. Carbon 32(4):735–741
17. Zhang Y et al (2011) Enhanced thermal conductivity in copper matrix composites reinforced with titanium-coated diamond particles. Script Mater 65(12):1097–1100
18. Powell R, Ho CY, Liley PE (1966) Thermal conductivity of selected materials. Vol. 8. 1966: US Department of Commerce, National Bureau of Standards Washington, DC
19. Gau C, Ko H, Chen H (2009) Piezoresistive characteristics of MWNT nanocomposites and fabrication as a polymer pressure sensor. Nanotechnology 20(18):185503
20. Kang JH et al (2009) Piezoresistive characteristics of single wall carbon nanotube/polyimide nanocomposites. J Polym Sci, Part B: Polym Phys 47(10):994–1003
21. Hu N et al (2011) Piezoresistive strain sensors made from carbon nanotubes based polymer nanocomposites. Sensors 11(11):10691–10723
22. Obitayo W, Liu T (2012) A review: carbon nanotube-based piezoresistive strain sensors. J Sens
23. Hu N et al (2008) Tunneling effect in a polymer/carbon nanotube nanocomposite strain sensor. Acta Mater 56(13):2929–2936
24. Wang L, Li Y (2012) A review for conductive polymer piezoresistive composites and a development of a compliant pressure transducer. IEEE Trans Instrum Meas 62(2):495–502
25. Sun X et al (2018) A highly-sensitive flexible tactile sensor array utilizing piezoresistive carbon nanotube–polydimethylsiloxane composite. J Micromech Microeng 28(10):105011
26. Can-Ortiz A, Abot J, Avilés F (2019) Electrical characterization of carbon-based fibers and their application for sensing relaxation-induced piezoresistivity in polymer composites. Carbon 145:119–130
27. Kingston C et al (2014) Release characteristics of selected carbon nanotube polymer composites. Carbon 68:33–57
28. Arash B, Wang Q, Varadan V (2014) Mechanical properties of carbon nanotube/polymer composites. Sci Rep 4:6479
29. Benson J et al (2013) Multifunctional CNT–polymer composites for ultra-tough structural supercapacitors and desalination devices. Adv Mater 25(45):6625–6632
30. Dalmas F et al (2005) Multiwalled carbon nanotube/polymer nanocomposites: processing and properties. J Polym Sci Part B: Polym Phys 43(10):1186–1197
31. Dufresne A et al (2002) Processing and characterization of carbon nanotube/poly (styrene-co-butyl acrylate) nanocomposites. J Mater Sci 37(18):3915–3923
32. Xiang D et al (2021) 3D-printed flexible piezoresistive sensors for stretching and out-of-plane forces. Macromol Mater Eng 2021:2100437
33. Thostenson ET, Chou T-W (2002) Aligned multi-walled carbon nanotube-reinforced composites: processing and mechanical characterization. J Phys D Appl Phys 35(16):L77
34. Meincke O et al (2004) Mechanical properties and electrical conductivity of carbon-nanotube filled polyamide-6 and its blends with acrylonitrile/butadiene/styrene. Polymer 45(3):739–748
35. Sandler J et al (2004) A comparative study of melt spun polyamide-12 fibres reinforced with carbon nanotubes and nanofibres. Polymer 45(6):2001–2015
36. Andrews R et al (2002) Multiwall carbon nanotubes: synthesis and application. Acc Chem Res 35(12):1008–1017
37. Velasco-Santos C et al (2003) Improvement of thermal and mechanical properties of carbon nanotube composites through chemical functionalization. Chem Mater 15(23):4470–4475
38. Zhao C et al (2005) Synthesis and characterization of multiwalled carbon nanotubes reinforced polyamide 6 via in situ polymerization. Polymer 46(14):5125–5132
39. Putz KW et al (2004) Elastic modulus of single-walled carbon nanotube/poly (methyl methacrylate) nanocomposites. J Polym Sci, Part B: Polym Phys 42(12):2286–2293
40. Byrne MT, Gun'ko YK (2010) Recent advances in research on carbon nanotube–polymer composites. Adv Mater 22(15):1672–1688
41. Coleman JN et al (2006) Small but strong: a review of the mechanical properties of carbon nanotube–polymer composites. Carbon 44(9):1624–1652
42. Coleman JN, Khan U, Gun'ko YK (2006) Mechanical reinforcement of polymers using carbon nanotubes. Adv Mater 18(6):689–706
43. Mamedov AA et al (2002) Molecular design of strong single-wall carbon nanotube/polyelectrolyte multilayer composites. Nat Mater 1(3):190–194
44. Olek M et al (2004) Layer-by-layer assembled composites from multiwall carbon nanotubes with different morphologies. Nano Lett 4(10):1889–1895
45. O'Connor I et al (2009) High-strength, high-toughness composite fibers by swelling Kevlar in nanotube suspensions. Small 5(4):466–469
46. O'Connor I et al (2009) Development of transparent, conducting composites by surface infiltration of nanotubes into commercial polymer films. Carbon 47(8):1983–1988
47. Endo M et al (2005) 'Buckypaper'from coaxial nanotubes. Nature 433(7025):476–476
48. Wang D et al (2008) Highly oriented carbon nanotube papers made of aligned carbon nanotubes. Nanotechnology 19(7):075609
49. Zhou Y, Hu L, Grüner G (2006) A method of printing carbon nanotube thin films. Appl Phys Lett 88(12):123109
50. Berhan L et al (2004) Mechanical properties of nanotube sheets: Alterations in joint morphology and achievable moduli in manufacturable materials. J Appl Phys 95(8):4335–4345
51. Chae HG et al (2005) A comparison of reinforcement efficiency of various types of carbon nanotubes in polyacrylonitrile fiber. Polymer 46(24):10925–10935
52. Mai F et al (2010) Superior reinforcement in melt-spun polyethylene/multiwalled carbon nanotube fiber through formation of a shish-kebab structure. J Phys Chem B 114(33):10693–10702
53. Mercader C et al (2012) Scalable process for the spinning of PVA–carbon nanotube composite fibers. J Appl Polym Sci 125(S1):E191–E196
54. Miaudet P et al (2007) Thermo-electrical properties of PVA–nanotube composite fibers. Polymer 48(14):4068–4074
55. Scaffaro R, Maio A, Tito A (2012) High performance PA6/CNTs nanohybrid fibers prepared in the melt. Compos Sci Technol 72(15):1918–1923
56. Zeng J et al (2004) Processing and properties of poly (methyl methacrylate)/carbon nanofiber composites. Compos B Eng 35(3):245–249

57. Anand KA et al (2010) PET-SWNT nanocomposite fibers through melt spinning. Int J Polym Mater 59(6):438–449
58. Kim J-W et al (2007) Characteristics of pitch-based carbon fibers containing multi-wall carbon nanotubes. J Ind Eng Chem 13(5):757–763
59. Andrews R et al (1999) Nanotube composite carbon fibers. Appl Phys Lett 75(9):1329–1331
60. Mottaghitalab V, Spinks GM, Wallace GG (2005) The influence of carbon nanotubes on mechanical and electrical properties of polyaniline fibers. Synth Met 152(1–3):77–80
61. Jose MV et al (2007) Polypropylene/carbon nanotube nanocomposite fibers: process–morphology–property relationships. J Appl Polym Sci 103(6):3844–3850
62. Teng N-Y, Dallmeyer I, Kadla JF (2013) Incorporation of multiwalled carbon nanotubes into electrospun softwood Kraft lignin-based fibers. J Wood Chem Technol 33(4):299–316
63. Jain R et al (2010) Processing, structure and properties of poly (ether ketone) grafted few wall carbon nanotube composite fibers. Polymer 51(17):3940–3947
64. Muñoz E et al (2005) Highly conducting carbon nanotube/polyethyleneimine composite fibers. Adv Mater 17(8):1064–1067
65. Khan WS, Asmatulu R, Eltabey MM (2013) Electrical and thermal characterization of electrospun PVP nanocomposite fibers. J Nanomater
66. Siochi EJ et al (2004) Melt processing of SWCNT-polyimide nanocomposite fibers. Compos B Eng 35(5):439–446
67. Saligheh O et al (2013) The effect of multi-walled carbon nanotubes on morphology, crystallinity and mechanical properties of PBT/MWCNT composite nanofibers. J Polym Res 20(2):1–6
68. Soroudi A, Skrifvars M (2010) Melt blending of carbon nanotubes/polyaniline/polypropylene compounds and their melt spinning to conductive fibres. Synth Met 160(11–12):1143–1147
69. Hooshmand S, Soroudi A, Skrifvars M (2011) Electro-conductive composite fibers by melt spinning of polypropylene/polyamide/carbon nanotubes. Synth Met 161(15–16):1731–1737
70. Xiang D et al (2020) Synergistic effects of hybrid conductive nanofillers on the performance of 3D printed highly elastic strain sensors. Compos Part A: Appl Sci Manuf 129:105730
71. Cheng H et al (2019) Synergetic effect of Fe3O4 nanoparticles and carbon on flexible poly (vinylidence fluoride) based films with higher heat dissipation to improve electromagnetic shielding. Compos A Appl Sci Manuf 121:139–148
72. Sohn K-S et al (2016) A mechanoluminescent ZnS: Cu/rhodamine/SiO2/PDMS and piezoresistive CNT/PDMS hybrid sensor: red-light emission and a standardized strain quantification. ACS Appl Mater Interfaces 8(50):34777–34783
73. Yoon SG, Chang ST (2017) Microfluidic capacitive sensors with ionic liquid electrodes and CNT/PDMS nanocomposites for simultaneous sensing of pressure and temperature. J Mater Chem C 5(8):1910–1919
74. Lai Y-T, Chen Y-M, Yang Y-JJ (2011) A novel CNT-PDMS-based tactile sensing array with resistivity retaining and recovering by using dielectrophoresis effect. J Microelectromech Syst 21(1):217–223
75. Wu L et al (2019) Screen-printed flexible temperature sensor based on FG/CNT/PDMS composite with constant TCR. J Mater Sci: Mater Electron 30(10):9593–9601
76. Du J et al (2020) Optimized CNT-PDMS flexible composite for attachable health-care device. Sensors 20(16):4523
77. Le H et al (2014) The role of linked phospholipids in the rubber-filler interaction in carbon nanotube (CNT) filled natural rubber (NR) composites. Polymer 55(18):4738–4747
78. Thomas PS et al (2012) Electrical properties of natural rubber nanocomposites: effect of 1-octadecanol functionalization of carbon nanotubes. J Mater Sci 47(7):3344–3349
79. Le H et al (2012) Kinetics of filler wetting and dispersion in carbon nanotube/rubber composites. Carbon 50(12):4543–4556
80. Jung S et al (2014) Reverse-micelle-induced porous pressure-sensitive rubber for wearable human–machine interfaces. Adv Mater 26(28):4825–4830
81. Xu M et al (2021) Breathable, degradable piezoresistive skin sensor based on a sandwich structure for high-performance pressure detection. Adv Electron Mater 7(10):2100368
82. Ellingford C et al (2019) Electrical dual-percolation in MWCNTs/SBS/PVDF based thermoplastic elastomer (TPE) composites and the effect of mechanical stretching. Eur Polymer J 112:504–514
83. Wang S et al (2021) In situ and intraoperative detection of the ureter injury using a highly sensitive piezoresistive sensor with a tunable porous structure. ACS Appl Mater Interfaces 13(18):21669–21679
84. Wang L et al (2020) Highly electrically conductive polymer composite with a novel fiber-based segregated structure. J Mater Sci 55(25):11727–11738
85. Zhang X et al (2020) Flexible and high-performance piezoresistive strain sensors based on carbon nanoparticles@ polyurethane sponges. Compos Sci Technol 200:108437
86. Chen X et al (2022) 3D printed high-performance spider web-like flexible strain sensors with directional strain recognition based on conductive polymer composites. Mater Lett 306:130935
87. Chen S et al (2021) Flexible Piezoresistive Three-Dimensional Force Sensor Based on Interlocked Structures. Sens Actuat A: Phys 2021:112857
88. Tran AV, Zhang X, Zhu B (2018) Mechanical structural design of a piezoresistive pressure sensor for low-pressure measurement: a computational analysis by increases in the sensor sensitivity. Sensors 18(7):2023
89. Zhang P et al (2019) Flexible piezoresistive sensor with the microarray structure based on self-assembly of multi-walled carbon nanotubes. Sensors 19(22):4985
90. Yang Q et al (2020) Performance evaluation of bitumen with a homogeneous dispersion of carbon nanotubes. Carbon 158:465–471
91. Simmons JG (1963) Low-voltage current-voltage relationship of tunnel junctions. J Appl Phys 34(1):238–239
92. Fisher J, Giaever I (1961) Tunneling through thin insulating layers. J Appl Phys 32(2):172–177
93. Wang L, Wang X, Li Y (2012) Relation between repeated uniaxial compressive pressure and electrical resistance of carbon nanotube filled silicone rubber composite. Compos A Appl Sci Manuf 43(2):268–274
94. Wang Z, Ye X (2014) An investigation on piezoresistive behavior of carbon nanotube/polymer composites: II. Positive piezoresistive effect. Nanotechnology 25(28):285502
95. Luheng W, Tianhuai D, Peng W (2009) Influence of carbon black concentration on piezoresistivity for carbon-black-filled silicone rubber composite. Carbon 47(14):3151–3157
96. Yi Y, Samara A, Wang B (2020) A new approach for an ultrathin piezoresistive sensor based on solidified carbon ink fil m. J Mater Sci 2020:1–8
97. Shindo Y et al (2012) Electrical resistance change and crack behavior in carbon nanotube/polymer composites under tensile loading. Compos B Eng 43(1):39–43
98. Sekitani T, Someya T (2010) Stretchable, large-area organic electronics. Adv Mater 22(20):2228–2246
99. Wang X et al (2014) Silk-molded flexible, ultrasensitive, and highly stable electronic skin for monitoring human physiological signals. Adv Mater 26(9):1336–1342

100. Yi Y, Chen J, Takahata K (2019) Wirelessly powered resonant-heating stent system: design, prototyping, and optimization. IEEE Trans Antennas Propag 68(1):482–490
101. Yi Y et al (2019) Wireless hyperthermia stent system for restenosis treatment and testing with swine model. IEEE Trans Biomed Eng 67(4):1097–1104
102. Yi Y et al (2019) Wirelessly Heating Stents via Radiofrequency Resonance toward Enabling Endovascular Hyperthermia. Adv Healthcare Mater 8(22):1900708
103. Loh KJ et al (2007) Multifunctional layer-by-layer carbon nanotube–polyelectrolyte thin films for strain and corrosion sensing. Smart Mater Struct 16(2):429
104. Kang I et al (2006) A carbon nanotube strain sensor for structural health monitoring. Smart Mater Struct 15(3):737